# Photoemission study of the surface electronic structure of W(001)

Greg S. Elliott, Kevin E. Smith, and Stephen D. Kevan
*Department of Physics, University of Oregon, Eugene, Oregon 97403*
(Received 29 October 1990; revised manuscript received 14 June 1991)

We report a high-resolution angle-resolved photoemission study of the surface electronic structure of the high-temperature phase of W(001). We have focused particularly upon the electron states within a few electron volts of the Fermi level in an attempt to characterize the interplay between the electronic and atomic structures of this surface. We relate these measurements of the surface band structure along the high-symmetry directions to the surface Fermi contours published recently. Most importantly, we observe a band to be located at or near the Fermi level over a sizable region of momentum space, approximately centered on the $\bar{\Sigma}$ line between $\bar{\Gamma}$ and $\bar{M}$. This feature is well placed to couple to phonon modes characteristic of the low-temperature $c(2\times2)$ structure observed on this surface. We find that the spin-orbit interaction has a profound influence on the topology of the bands that are involved in driving the surface to reconstruct. The relationship of these results to existing calculations, to the wave vector of the reconstruction, and to recent measurements of surface phonon-dispersion relations will be discussed.

## I. INTRODUCTION

The phenomenon of surface reconstruction, wherein a surface has a lower symmetry than that expected from a simple termination of the bulk crystal, has fascinated surface physicists for many years. Prototypical clean surface reconstructions are observed on W(001) (Ref. 1) and Mo(001) (Ref. 2) below room temperature, which form $c(2\times2)$ and $(7\sqrt{2}\times\sqrt{2})R_{45}°$ structures,[3,4] respectively. These reconstructions have been extensively studied both by computations[5–19] and by a variety of surface techniques.[20–33] The local geometric arrangement of the surface atoms is thought to be similar on the two surfaces, i.e., zigzag chains of atoms oriented along the [110] azimuthal direction. However, there is no concensus concerning the precise mechanism which forces the reconstructions to occur. The difference in unit cell size between these two otherwise similar surfaces is indicative of the difficulty of attaining a general understanding of this mechanism. The ground state must result from a delicate interplay between localized and delocalized electronic interactions.

Early theories postulated that these reconstructions were driven by a charge-density-wave instability related to nested segments of the surface Fermi contours.[5–8] In other words, a mechanism involving delocalized electronic band states was proposed. These theories, which are similar to those which have been so successful in explaining the reconstructive behavior of quasi-one-dimensional (1D) and -2D metals,[34] explained the different unit cell sizes with ease. The wave vector of the reconstruction is related to a vector spanning one or more segments of the surface Fermi contours so that a reconstruction of arbitrary wave vector could result. Unfortunately, a determination of the W(001) surface Fermi contours found insufficient nesting to produce the necessary singularity in the electronic susceptibility to drive the reconstruction.[24] An alternative model based upon local bonding interactions and involving short-range Jahn-Teller-like forces was proposed and gained favor.[6,12,13,24,25] This local model has recently been shown to reproduce all behaviors observed on the W(001) surface.[35] It has thus provided a wealth of intuition concerning the structural stability of these surfaces. The local model is less easily applied to understand the large unit cell observed on Mo(001) since purely short-range forces might be expected to produce a relatively small repeat distance.

Recently, the impact of delocalized interactions has gained renewed support. This has come from nearly-first-principles calculations of both Mo(001) and W(001) which exhibit mode softening and hence reconstruction,[19] and also from elastic and inelastic helium scattering measurements on both surfaces.[28,29] Two helium-atom diffraction experiments on W(001) observed that the superlattice diffraction peaks shift away from the commensurate positions above room temperature. Inelastic helium-atom scattering measurements have produced surface phonon dispersion relations which exhibit softening of a phonon branch near, but not precisely at, the $\bar{M}$ point of the surface Brillouin zone (SBZ).[29] These data suggest that the first wave vector to soften is displaced from that characterizing the commensurate $c(2\times2)$ structure. The incommensurate diffraction pattern above room temperature has not been observed by low-energy electron,[1] x-ray,[30] and neon-atom[32] diffraction. The interpretation of the helium-atom diffraction results has been called into question from a careful consideration of the static factor of the surface,[36] but the parameters used to produce shifting superlattice peaks are apparently unphysical.[37] The more recent calculation[35] reproduces the helium scattering results by considering dynamical effects upon the structure factor. The structure of the high-temperature phase of W(001) is still subject to debate, but there is some experimental evidence for incommensurability and thus longer-ranged interactions on this surface.

While both models provide useful intuition, it is likely

 

that neither the localized nor the delocalized paradigm is strictly applicable. A fundamental understanding will come from a complete characterization of the electronic structure of these surfaces, particularly of those states close to the Fermi level ($E_F$). There have been several first-principles calculations[5–19] and angle-resolved photoemission studies[21–25] of the W(001) surface electronic structure. Unfortunately, there are discrepancies between the calculations and the experiments at energies near $E_F$ in regions of momentum space which are crucial to understanding the reconstruction. Moreover, there are discrepancies between the different experimental results.[24,25]

For this reason, we have undertaken such studies for both W(001) and Mo(001).[38] A preliminary accounting of our results for W(001) was reported previously.[33] We present a more detailed analysis of these data here. A primary conclusion from our work is that both paradigms have some element of validity, and thus both provide some useful intuition concerning the stability of these surfaces. Our surface-band dispersions are generally consistent with the limited dispersions reported in one of the previous experiments,[25] although our data set is more complete and our specific interpretations differ in some important respects. Our bands produce surface Fermi contours[33] which are significantly different from those reported earlier.[24] We deduce the importance of a particular feature in the Fermi contours, actually a diffuse band of states located very close to $E_F$ near the midpoint of the $\bar{\Sigma}$ line, in driving the reconstruction.

The structure of this paper is as follows. The next section describes our experimental techniques. Section III presents our experimental results and compares these to previous experiments and calculations. Section IV discusses our results in a broader context as they relate to surface reconstruction. The final section provides a brief summary.

## II. EXPERIMENTAL PROCEDURES

The experiment was carried out at the National Synchrotron Light Source at Brookhaven National Laboratory, using light from the 750-MeV storage ring, a 6-m toroidal grating monochromator,[39] and a high-resolution angle-resolving electron spectrometer which has been described previously.[40] For the experiments presented here, the total instrumental resolution was always less than 100 meV (full width at half maximum), and the full angular acceptance was 1° or better. Spectra could be accumulated with an adequate signal-to-noise ratio under these conditions in typically 2–5 min.

The tungsten crystal 8 mm in diameter was oriented along the [001] bulk crystalline axis by Laue backreflection to within 0.1°. A 0.5-mm-thick slice was cut and mechanically polished while maintaining the surface orientation. Three 0.5-mm-diameter holes were spark eroded along the edge of the sample, from which the sample was suspended on tungsten wires. The sample was heated by electron bombardment, and the surface temperature measured with an optical pyrometer. Initial cleaning was achieved *in vacuo* by repetitive cycles of oxidation at 1400 K in $5\times10^{-8}$ Torr $O_2$ followed by flashing to 2500 K every few minutes. A few hours of this procedure were required to deplete the sample of bulk carbon impurities, until a clean Auger spectrum was consistently observed following high-temperature flashes. The operating pressure of $(0.8-1.2)\times10^{-10}$ Torr was sufficient to maintain a clean surface for 15–20 min, as determined by the gradual disappearance of some of the more contamination-sensitive features in our photoemission spectra. These features were easily restored by thermally desorbing the residual hydrogen and carbon monoxide from the surface, which in practice was done after taking 2 or 3 spectra. This desorption procedure could be performed repeatedly for several days without degradation of the surface. Where required to determine the surface sensitivity of certain spectral features, the room-temperature surface was exposed to hydrogen gas in the form of $H_2$, either by back-filling the chamber or by placing the sample in the line of sight of a channel plate array doser.

## III. EXPERIMENTAL RESULTS

We start with a general presentation of our results, and then provide a more detailed description and analysis in the following sections. Our studies involved accumulat-

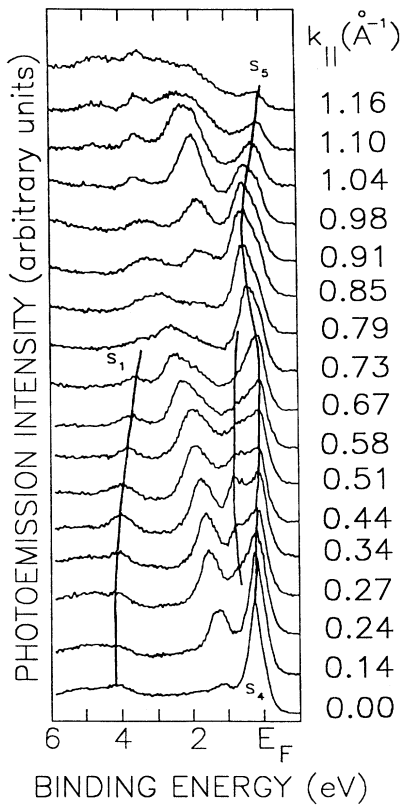


FIG. 1. ARP spectra of clean W(001) collected with the electron emission direction and the photon polarization vector in the same $\bar{\Sigma}$ mirror plane, at a photon energy of 20 eV, as a function of parallel momentum measured from $\bar{\Gamma}$ to $\bar{M}$ along $\bar{\Sigma}$.

ing over 2000 angle-resolved photoemission (ARP) spectra from the clean and hydrogen-contaminated W(001) surface. The experimental goal was to determine which spectral features could be associated with bulk states, which with surface states, and which with surface resonances, and then to map the surface-band dispersion relations. We followed the normal procedure[41–44] in such experiments of initially determining which features were particularly sensitive to contamination and which did not exhibit significant dispersion with the component of momentum normal to the surface, as would be expected for a two-dimensional state. The states which were determined to be surface levels were compared with a projection of the calculated bulk band structure normal to the surface to determine whether they were associated with a band gap. This comparison with a calculated ground-state projection is not without problems, since photoemission measures an excited quasiparticle state.[45] We find the projections to be useful guides in interpreting our data since the contours of the calculated projected gaps will be qualitatively correct.

Figures 1, 2, and 3 give a sampling of our photoemission spectra from clean W(001) along the $\bar{\Sigma}$, $\bar{\Delta}$, and $\bar{Y}$ lines of the SBZ, respectively. We have indicated with vertical curved lines the dispersion of features passing the aforementioned tests to determine surface character. For ease of reference below, these have been labeled $S_1$–$S_7$ in Figs. 1–4. The dispersion relations of these surface features are plotted in Fig. 4 on a projection of the tungsten bulk band structure onto the unreconstructed W(001) SBZ. The bulk bands in Fig. 4 were calculated using a Slater-Koster three-center nonorthogonal tight-binding interpolation scheme fitted to an augmented-

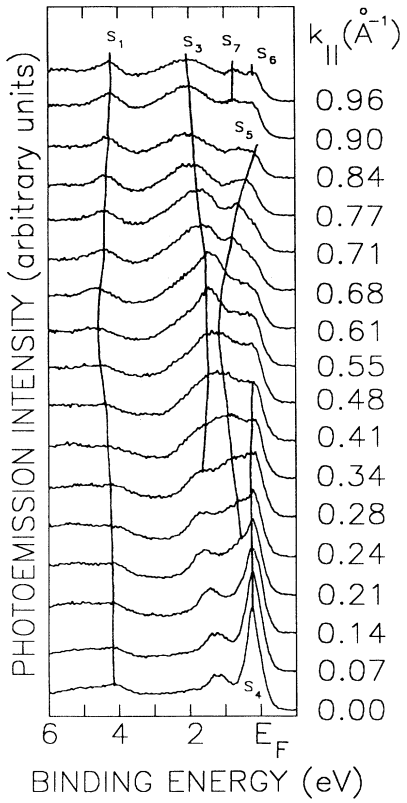


FIG. 2. ARP spectra of clean W(001) collected with the electron emission direction and the photon polarization vector in perpendicular $\bar{\Delta}$ mirror planes, at a photon energy of 20 eV, as a function of parallel momentum measured from $\bar{\Gamma}$ to $\bar{X}$ along $\bar{\Delta}$.

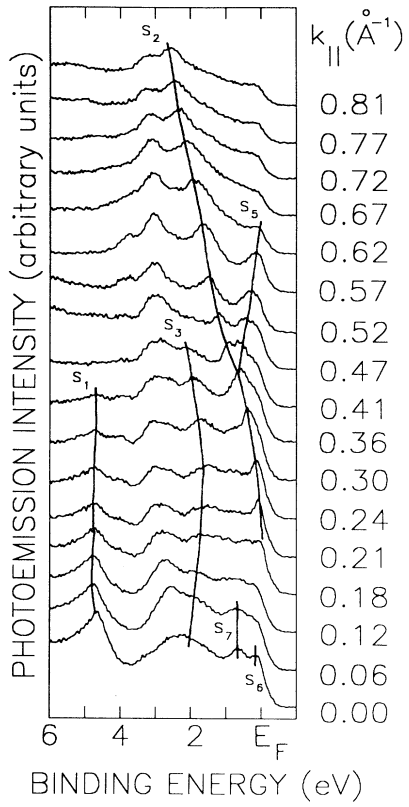


FIG. 3. ARP spectra of clean W(001) collected along the $\bar{Y}$ direction, at a photon energy of 20 eV, as a function of parallel momentum measured from $\bar{X}$ to $\bar{M}$ along $\bar{Y}$.

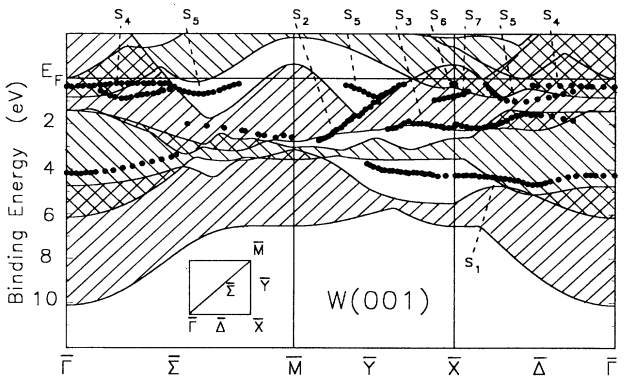


FIG. 4. Bulk tungsten band structure projected onto the (001) surface Brillouin zone, with the projected region for each band separately cross-hatched. The calculation includes the spin-orbit interaction, as explained in the text. The experimental points show the dispersions of the surface-localized states labeled $S_1$–$S_7$ in Figs. 1–3.

plane-wave band structure.[46] This interpolation scheme was modified as described elsewhere[41] to include the spin-orbit interaction, which was approximated with energy-independent W 5*d* and W 6*p* spin-orbit parameters taken from atomic energy level tables.[47] The unreconstructed W(001) surface is of 4 mm symmetry, and thus has two mirror symmetry lines, labeled $\bar{\Sigma}$ and $\bar{\Delta}$ in Fig. 4. The spin-orbit interaction breaks the mirror plane symmetry of the associated electronic states, so that separation of even- and odd-symmetry projections is not necessary.

Bulk tungsten has six valence electrons. Bands one and two are fully occupied. The lowest measured surface feature appears to split from band one, although it is often resonant with band two. This band has been adequately characterized elsewhere[21–25] and will not concern us here. The next two highest surface features appear to be related to bands two and three; one of them lies close to or in a projected gap along $\bar{Y}$. These bands are discussed further in Sec. III A. Bulk bands three and four are both partially occupied. There is a large projected gap between these two centered at $\bar{M}$. We observe a complex set of surface bands in and near this gap. These bands and their relation to the previously published Fermi contours are discussed in detail in Sec. III B. Two newly observed surface bands, $S_6$ and $S_7$, are described in Sec. III C. Our results are compared to previous experimental results and to existing calculations throughout Sec. III.

### A. Surface bands $S_2$ and $S_3$

We observe two bands, labeled $S_2$ and $S_3$ in Fig. 4, which appear to be predominantly associated with the second and third bulk bands. These both are most clearly visible along the $\bar{Y}$ azimuth, although they extend somewhat along the other symmetry directions. Along $\bar{Y}$, $S_2$ disperses rapdily upward from $\bar{M}$ toward $\bar{X}$. This band is a resonance through much of its dispersion. $S_2$ approaches bands $S_5$ and $S_6$ at the top of its dispersion; this will be discussed further below. The only previous experimental study which presented surface-band dispersions along $\bar{Y}$ distinguished just one band; this was in fairly good accord with our results for $S_2$.[24] Calculated bands along $\bar{Y}$ also show just one band in this energy region, and the calculated dispersion relation corresponds most closely, although imperfectly, with that of $S_2$.[9]

$S_3$ is observed to exist in or near a projected gap along $\bar{Y}$ between bands 2 and 3. As is the case for $S_1$, this band disappears from our spectra near $\bar{M}$, presumably due to the complexity of the bands in this vicinity. Along $\bar{\Delta}$, $S_3$ disperses upward away from the $\bar{X}$ point, and approaches bands $S_4$ and $S_5$. In the absence of the spin-orbit interaction, the projected gap along $\bar{Y}$ between bands 2 and 3 would close at the $\bar{X}$ and $\bar{M}$ points. Thus $S_3$ is necessarily a resonance along these lines. The gap along $\bar{Y}$ is narrow and would presumably support a state with a fairly long decay length into the bulk. This could explain why $S_3$ has been neither predicted by finite slab calculations nor observed in previous experimental studies using a small photon energy range.[24]

### B. Surface bands $S_4$ and $S_5$

The bands labeled $S_4$ and $S_5$ have been the focus of much experimental and theoretical study in the past, since they are located near $E_F$ and can thus impact the surface reconstruction. The Fermi level of bulk tungsten lies in a broad minimum in the electronic desnity of states located between the predominantly bonding $t_{2g}$ and antibonding $e_g$ 5*d* manifolds. Strong hybridization leads to a complex array of projected band gaps and surface levels. The gaps in this region are at the heart of the localized-delocalized debate, since, if the gap were absolute and tungsten were a semiconductor, the local bonding model would almost certainly be a reasonable construct.

#### *1. Dispersion relations for bands $S_4$ and $S_5$*

Determining reliable dispersion relations for bands $S_4$ and $S_5$ has proven particularly troublesome in essentially all previous experiments and calculations. These bands are resonances through much of the SBZ, and are also strongly hybridized with each other. Moreover, as indicated below and elsewhere,[10,33] the spin-orbit interaction has a profound impact on these bands. The assignment of individual surface bands near $E_F$ is arbitrary in some regions of the SBZ due to some uncertainties regarding band connectivity.

Along $\bar{\Delta}$ near zone center, we observe the well-known "Swanson hump" (SH) feature,[20] labeled $S_4$ in Fig. 4. This band disperses monotonically toward $E_F$ as $k_\parallel$ is moved away from zone center, and it vanishes near $k_\parallel = 0.5$ Å$^{-1}$. Near $k_\parallel = 0.25$ Å$^{-1}$, $S_5$ splits off below $S_4$ and disperses downward. Half way across the SBZ, $S_5$ approaches $S_3$ which is dispersing upwards away from the $\bar{X}$ point. Spectra from this region are quite complex, and the results are dependent upon the photon polarization and energy used. In some scans, $S_5$ and $S_3$ appear to hybridize, leaving an avoided crossing $\sim 0.3$ eV wide. In others, one of the two bands is much more intense than the other. Since the intensity is passed from one band to the other through the hybridization region, the avoided crossing is not easily visible. Figure 4 displays these results as avoided crossings, but in actual fact the results are ambiguous.

On the zone center side of the avoided crossing, the peak corresponding to $S_3$ slowly loses its surface character as it disappears into the continuum formed by bands 2 and 3. Toward the zone boundary, $S_5$ disperses back to lower binding energy, and crosses $E_F$ at $k_\parallel = 0.86$ Å$^{-1}$. This Fermi contour was followed around the $\bar{X}$ point,[33] and $S_5$ was found to be continuous with the band dispersing downward through $E_F$ away from $\bar{X}$ along the $\bar{Y}$ direction. Continuing along $\bar{Y}$ toward $\bar{M}$, $S_5$ first approaches $S_2$ and then changes direction and crosses $E_F$ roughly two-thirds of the way to $\bar{M}$. Again, this Fermi contour was followed around $\bar{M}$, and $S_5$ crosses the $\bar{\Sigma}$ line about 20% of the way to $\bar{\Gamma}$. After crossing below $E_F$ away from $\bar{M}$ along $\bar{\Sigma}$, $S_5$ disperses downward briefly, and then changes direction to head back toward $E_F$.

Roughly half-way to $\bar{\Gamma}$ along $\bar{\Sigma}$, the connectivity of

bands $S_4$ and $S_5$ becomes difficult to ascertain. Near zone center, only the SH, labeled $S_4$ above, is seen. For $0.2\ \text{Å}^{-1} < k_{\parallel} < 0.7\ \text{Å}^{-1}$, a band splits to higher binding energy, while the feature derived from the SH remains very close to $E_F$ for several spectra. Indeed, the binding energy of the SH feature is comparable to its width, so that a reliable binding energy cannot be deduced other than to say that it is less than 0.2 eV. Meanwhile, the deeper band appears to lose some intensity before the two features merge near $k_{\parallel} < 0.7\ \text{Å}^{-1}$. Further out along $\bar{\Sigma}$, the remaining single feature disperses to higher binding energy, changes direction, and crosses $E_F$ at $k_{\parallel} = 1.19\ \text{Å}^{-1}$ which we assigned as $S_5$ above.

Note that the spectra in Fig. 1 were collected with the electron emission direction and the photon polarization vector on opposite sides of the surface normal. This can and does produce spectra with peak intensities substantially different from the conventional orientation with the polarization vector and the emission vector on the same side of normal. In other polarizations, the connectivity of the SH band and the $S_5$ Fermi-level crossing is not as apparent as appears to be the case in Fig. 1.

The most consistent connectivity for $S_4$ and $S_5$ is to assign the band which splits off below the SH as $S_5$ along both $\bar{\Delta}$ and $\bar{\Sigma}$. This conclusion was verified with scans off the $\bar{\Sigma}$ and $\bar{\Delta}$ mirror planes where $S_5$ was clearly visible so that the connectivity could be established. We acknowledge some ambiguity in this assignment along $\bar{\Sigma}$, in view of the spectra in Fig. 1. The region along $\bar{\Sigma}$ of $0.3 < k_{\parallel} < 0.7\ \text{Å}^{-1}$ is spectrally complex, and the bands near $E_F$ are not easy to assign. It is not really even clear whether $S_4$ crosses $E_F$ one or more times somewhere in this region; the sensitivity of the ARP technique is not adequate to address this issue.

Along $\bar{\Sigma}$ and $\bar{Y}$, $S_5$ lies in and mimics a large projected gap near the $\bar{M}$ point of the SBZ. Both the gap and the surface band are nearly isotropic about $\bar{M}$. Parabolic extrapolation of our band from the Fermi level yields a band origin 0.25 eV above the $E_F$ with an effective mass 0.8 times the free-electron mass. A recent inverse photoemission study locates a surface band at $\bar{M}$ which appears to have the correct dispersion relation to be identified with our $S_5$.[26] The results of another inverse photoemission study are quite different from the first, and no band comparable to $S_5$ was identified.[27].

A similar relationship between $S_5$ and the projected bulk bands is approximately observed near $\bar{X}$. In this case, however, $S_5$ is degenerate with the projection of bulk band 4. Moreover, the dimension of the surface hole pocket is comparable to that of the projection of the bulk hole ellipsoid at $\bar{X}$.[33] Thus the surface orbit may be a resonance degenerate with the third bulk band edge. By extrapolation, we predict a band origin 0.45 eV above $E_F$ at $\bar{X}$, with effective masses of 0.2 and 0.5 times the free electron mass along $\bar{\Delta}$ and $\bar{Y}$, respectively.

$S_5$ forms closed Fermi contours around both the $\bar{X}$ and the $\bar{M}$ points.[33] Both of these contours are hole pockets in the sense that they surround unoccupied states. Also, both are clearly associated with the projection of the hole ellipsoid in the bulk Fermi surface.[48] This association of a surface Fermi contour with a particular feature in the projected Fermi surface is very similar to previous observations on W(011),[41] Mo(011),[41] Pd(001),[49] and Pt(111).[50] We included in Fig. 3 of Ref. 33 a shaded region centered on the $\bar{\Sigma}$ line corresponding to where $S_4$ is too close to $E_F$ to measure its binding energy reliably. While this is not precisely a Fermi contour, the close proximity of $S_4$ to $E_F$ implies a potentially significant impact upon the generalized susceptibility of the surface.

### 2. *Comparison to previous experimental results*

The only other experimental study which attempted to be as complete as the one reported here[24] produced bands which are significantly different from ours. That study utilized radiation from a resonance lamp, a procedure which limits the photon energies available and which also tends not to be as reliable as synchrotron radiation in maintaining a clean surface.

Our results are consistent with a more limited study which focused only upon the bands along $\bar{\Sigma}$.[25] The spectra reported there were qualitatively similar to those we have observed. The Fermi level crossing along $\bar{\Sigma}$, for example, is nearly identical to ours. Our higher resolution and more complete analysis leads to a different conclusion about the precise dispersion relations near the middle of the $\bar{\Sigma}$ line, but otherwise the studies are broadly consistent. Given the uncertainty inherent in interpreting spectra such as those presented in Fig. 1, we take this agreement to mean that experiments have converged upon a common result with which calculations can be compared.

### 3. *Comparison to previous computational results*

Existing scalar relativistic calculations provide a poor representation of our experimental results for $S_4$ and $S_5$.[7,9–14] For example, the size of the hole pocket about $\bar{M}$ is significantly overestimated, and the shape of the pocket is not predicted to be as isotropic as we observe. The hole pocket we observe around $\bar{X}$ and the portion of $S_5$ which forms it have not been predicted, perhaps because of this band's resonance character. The character of the hole pocket centered on $\bar{M}$ and its associated band along $\bar{\Sigma}$ have been the subject of intensive study in the past. The reason for this interest is that the observed $c(2\times2)$ reconstruction is characterized by a wave-vector parallel to $\bar{\Sigma}$ with a length equal to the distance from $\bar{\Gamma}$ to $\bar{M}$. Several calculations place the crossing for this hole pocket roughly half-way from $\bar{\Gamma}$ to $\bar{M}$, and an apparent connection to the reconstruction was thus proposed.[8,9,14] The calculated hole pocket is formed by the odd-symmetry component of a doublet of surface bands which have similar dispersion relations along $\bar{\Sigma}$. Our results are inconsistent with this band topology.

One reason why our results may not be matched by theory is that essentially all calculations have been performed on an ideal $(1\times1)$ surface, while our experiments have been performed on the room-temperature phase which almost certainly is not an ideal bulk termination. The fact that the ordered phase develops below 250 K

suggests, but does not prove, that the modifications to the electronic structure induced by reconstruction will be small (on the scale of $k_B T \sim 20$ meV). By comparison, the discprepancies butween our results and scalar relativistic calculations are topological and cannot be explained by small perturbations and Brillouin zone folding.

Another concern in comparing photoemission results with those of calculations is that photoemission measures an excited state, while the ground state is normally calculated. This problem usually leads to calculated bands which are qualitatively correct, but quantitatively wrong: the calculated band gaps are too small, the bandwidths are too large, etc.[45] The fact that our dispersions are generally not even qualitatively matched by scalar relativistic calculations indicates that this is probably not the dominant source of the discrepancy.

#### *4. Impact of the spin-orbit interaction*

The gap in Fig. 3 along $\bar{\Sigma}$ near $E_F$ results from the superposition of a large gap of odd symmetry with a narrower gap of even symmetry.[10] Scalar relativistic calculations predict that each of these gaps supports a surface state; these form the doublet mentioned above. Within 1 eV of $E_F$, the calculated even- and odd-surface band dispersion relations are nearly coincident. In this circumstance, these bands will be strongly hybridized by the spin-orbit interaction. Due to the large atomic spin-orbit parameter in a 5*d* metal, the resulting dispersion relations will bear little semblance to those in the scalar relativistic calculation. Attention has also been focused upon the mirror plane symmetry of the electronic states necessary to produce the observed reconstruction.[6–19,24,51] For $S_4$ and $S_5$ we have not observed behaviors consistent with any particular mirror plane symmetry. If we mentally hybridize the calculated odd- and even-symmetry bands such that one shifts up and the other shifts down by energies on the order of 5*d* spin-orbit parameter, two bands of strongly mixed symmetry result, one in the middle of the fully relativistic gap, and another which may or may not even cross $E_F$. This is very close to what we observe for $S_4$ and $S_5$. In particular, the spin-orbit interaction plays a key role in producing the observed dispersion relation of $S_4$, with its unusual flat region near $E_F$ along $\bar{\Sigma}$.

A recent calculation included the spin-orbit interaction in a partially self-consistent way.[10] The size of the hole pocket around $\bar{M}$ was reduced somewhat relative to the scalar relativistic result, although not to the level observed in the present study. While the continuity of the surface bands was difficult to distinguish due to the finite size of the calculated tungsten slab, our dispersion relations for $S_4$ and $S_5$ are qualitatively consistent with this calculation. We take this qualitative match to mean that calculations which do not include the spin-orbit interaction are seriously flawed in their treatment of surface bands near $E_F$. This spin-orbit-induced hybridization apparently has a profound impact upon the $c(2\times2)$ reconstruction.

"Second-order" calculations have been undertaken in order to model the dynamical behavior of the surface layers.[18,19,35] In all of these cases, however, the scalar relativistic bands were used as input to produce, for example, parameters in model Hamiltonians. In view of the discord between experimental and calculated bands and Fermi contours, these second-order calculations, while undoubtedly providing useful intuition, are currently imcomplete. Calculations which model surface dynamical properties should be undertaken using the parametrization which includes the spin-orbit interaction.

### C. Surface bands $S_6$ and $S_7$.

Results along $\bar{\Delta}$ for the surface bands $S_6$ and $S_7$ near $\bar{X}$ are also obtained. While these states are probably not directly associated with the reconstruction, their existence provides another useful test for future computations. The region near $E_F$ in Fig. 2 is unusually complex in the vicinity of $\bar{X}$. $S_6$ appears as a very sharp feature essentially at $E_F$ over only a small region of the SBZ. Figure 3 indicates that $S_6$ is resonant with both bands 3 and 4. We interpret these observations in terms of a surface band which disperses below $E_F$ near $\bar{X}$ to form a small electron pocket in the Fermi contours. This pocket appears to be loosely associated with the intersection of the tips of the projections of the bulk electron jacks in the first and second SBZ.[33] Like $S_6$, $S_7$ is observed in Fig. 2 over a fairly small region of the SBZ near $\bar{X}$. Away from $\bar{X}$ along both the $\bar{\Delta}$ and $\bar{Y}$ lines, $S_7$ becomes diffuse so that the dispersion relation cannot be mapped. In Fig. 3, it is tempting to connect $S_7$ with $S_2$ along $\bar{Y}$, although we have no spectral evidence for this.

## IV. CLEAN SURFACE RECONSTRUCTION

### A. The localized and delocalized paradigms

The character of the clean surface reconstruction implies substantial nonadiabaticity. That is, the Born-Oppenheimer approximation is not strictly valid in treating this system. The localized and delocalized driving mechanisms for the reconstruction mentioned in the Introduction constitute the simplest conceptual models for treating these nonadiabatic interactions. The local bonding model is related to nonadiabatic interactions in molecular systems which are modeled by the dynamical Jahn-Teller effect.[52] On W(001), the localized mechanism normally is based upon the existence of a large peak in the surface density of states $E_F$ composed of weakly interacting dangling bond orbitals caused by forming the surface.[17] The simplest model embodying nonadiabatic effects in the delocalized picture is the aforementioned Peierls or charge-density-wave (CDW) distortion.[53] In this case, electron and hole states on opposite sides of the Fermi surface are coupled by a particular phonon mode having a well-defined wave vector.

The underlying physics of these two paradigms is similar; the differences lie primarily in how one chooses to conceptualize a basis set in solving an electronic Hamiltonian. This similarity can be described using an expression derived in the random phase approximation for the wave vector and frequency-dependent generalized susceptibility of a solid $\chi^0(\mathbf{q},\omega)$. Ignoring matrix element

effects and considering only a single band, this is given by[54]

$$\chi^0(\mathbf{q},\omega)=\sum_k \frac{f(\mathbf{k})-f(\mathbf{k}+\mathbf{q})}{E(\mathbf{k}+\mathbf{q})-E(\mathbf{k})-\hbar\omega}\ , \tag{1}$$

where $f(\mathbf{k})$ is the Fermi function for state $\mathbf{k}$, $E(\mathbf{k})$ is the energy of state $\mathbf{k}$, and the sum is over all bands in the first Brillouin zone. The energy difference in the denominator can lead to near-singularities in the susceptibility. These in turn can lead to formation of a spin- or charge-density-wave ground state characterized at small $\omega$ by a wave vector which exactly spans the Fermi surface.[34,55,56]

The strength of the singularities in $\chi^0(\mathbf{q},\omega)$ are related both to the size of the vibronic coupling matrix elements [which were ignored in Eq. (1)], and to the size of the regions in $\mathbf{k}$ space which are effectively coupled by a given wave vector. Aside from symmetry effects, our experiment cannot provide information on the matrix elements. By contrast, a qualitative estimate can be made of the size of the coupled regions. This size is determined by two factors, the first related to the delocalized, Peierls-like mechanism and the second to the localized, Jahn-Teller-like mechanism. The first requires efficient nesting of Fermi contours. That is, in two dimensions, the singularities are enhanced by coupled Fermi surface contours which have parallel tangents and similar curvatures. This simple geometrical construction is a generalization of the simple 1D Peierls model.[34] The second way in which the size of the coupled regions can be expanded is by coupling nearly dispersionless bands. This is synonymous with the condition that the Fermi velocity of the coupled states is comparable to nuclear velocities, so that the response of the electron gas to nuclear motion cannot be approximated as instantaneous. With dispersionless bands, there is a relatively large region over which bands disperse within $k_BT$ of $E_F$ so that the denominator in Eq. (1) remains small while the numerator remains finite. Flat bands imply localized states and large peaks in the local density of states, so this effect leads naturally to the localized paradigm.

### B. Surface electronic structure and the $c(2\times2)$ reconstruction

The bands which cross $E_F$ in Fig. 4 near the $\bar{X}$ and $\bar{M}$ points of the SBZ are reasonably well nested and might be expected to lead to significant singularities in the static susceptibility.[54] However, the coupled wave vectors are far from the wave vector of the observed reconstruction. The band has a Fermi velocity $v_F\sim1$ eV/Å$^{-1}$, which is much larger than typical nuclear velocities. The second mechanism related to localized interactions contributes little to any supposed nonadiabaticity. Interactions associated with the hole pockets fail to cause the surface to reconstruct due to the relatively large Fermi velocity and the resulting small number of states contributing to the susceptibility anomaly near nested wave vectors. In the terminology of a Peierls distortion, the stabilization energy gained through formation of CDW-like gaps in the electronic manifold is too small to overcome the lattice deformation energy.

The regions of the $\bar{\Sigma}$ lines where $S_4$ is very close to $E_F$ are very well nested, since the edges of the shaded regions in the Fermi surface are perpendicular to the associated $\bar{\Sigma}$ axis. Moreover, the band velocity is very small throughout the region. Both of these factors will contribute to a strong breakdown in adiabaticity and thus possibly to reconstruction. The localized and delocalized paradigms are also nicely unified in this way: the shaded region is partially delocalized in momentum space, implying partial localization in real space. The flat band would lead to a large peak in the local density of states near $E_F$, a prerequisite for applying the localized paradigm. If one assumes rough symmetry about $E_F$, the flat region of $S_4$ would produce a substantial peak in the surface density of states near $E_F$ with a width of 0.4–0.5 eV. This is in striking accord with recent first-principles calculations which have supported a local mechanism.[17] The existence of this large density of states may ultimately be the reason that local-bonding models have been successful in predicting surface properties. Much useful intuition has been gained from this work, since it is easier to think in terms of real-space, directed orbitals than momentum space couplings when considering surface reconstruction.

The primary complicating factor in associating the driving force for the reconstruction to the delocalized paradigm is that the commensurate wave vector, $q=1.41$ Å$^{-1}$ parallel to $\bar{\Sigma}$, is not precisely included within the set of vectors spanning flat regions of $S_4$ on opposite sides of the zone center. More precisely, the minimum and maximum wave vectors coupling these regions are given by 0.62 and 1.28 Å$^{-1}$, respectively. In a simple analysis, one might thus expect to observe an incommensurate surface, as suggested by the recent helium-atom scattering experiments above room temperature.[28,29] The ground state of Mo (001) is a long-range commensurate structure[3,4] and our results for that surface are generally compatible with the observed wave vector of the reconstruction.[38] As the driving forces for the two reconstructions must surely be similar, we believe that the shaded regions do in fact play a key role in driving the W(001) to reconstruct.

A possible explanation for the ambiguity between the range of nested wave vectors and that of the reconstruction lies in momentum-dependent electron-phonon coupling matrix elements. These are neglected in Eq. (1), but have been shown in calculations to be important. Specifically, recent calculations on the W(001) and Mo(001) reconstructions[19] suggested that the matrix elements shift the singularity in the susceptibility away from the incommensurate nesting vector and toward the commensurate one. This is actually another way to say that local interactions cannot be neglected, and that their impact appears through short-range interactions in the electron-phonon matrix elements.

While there are important details which are not matched by first-principles calculations, we see that our results are broadly consistent with both the localized and delocalized paradigms. Both contribute to the nonadiabaticity and to instability of the $(1\times1)$ surface.

## V. SUMMARY AND CONCLUSIONS

We have described a high-resolution angle-resolved photoemission study of the surface electronic structure of the high-temperature phase of W(001). Our results are in good accord with a more limited previous experiment, but are not well matched by existing scalar relativistic calculations. We described a band located at or near the Fermi level over a sizable region of the SBZ approximately centered on the $\bar{\Sigma}$ line, and discussed its relation to the low-temperature $c(2\times2)$ structure. The importance of the spin-orbit interaction was emphasized, and its role in the driving force for the reconstruction investigated.

## ACKNOWLEDGMENTS

This work was carried out in part at the NSLS at Brookhaven National Laboratory which is supported by the U.S. Department of Energy, Division of Materials Science and Division of Chemical Sciences. Financial support for this work was also provided by the USDOE under Grant No. DE-FG06-86ER45275. S.D.K. gratefully acknowledges partial support from the NSF and the Alfred P. Sloan Foundation.

[1]M. K. Debe and D. A. King, Phys. Rev. Lett. **39**, 708 (1977); J. Phys. C **10**, L303 (1977); Surf. Sci. **81**, 193 (1979); J. Phys. C **15**, 2257 (1982).
[2]T. E. Felter, R. A. Barker, and P. J. Estrup, Phys. Rev. Lett. **38**, 1138 (1977); R. A. Barker, P. J. Estrup, F. Jona, and P. M. Marcus, Solid State Commun. **25**, 375 (1978).
[3]E. Hulpke and D.-M. Smilgies, Phys. Rev. B **43**, 1260 (1991).
[4]T. Felter, J. Vac. Sci. Technol. A **9**, 1604 (1991).
[5]E. Tosatti, Solid State Commun. **25**, 637 (1978).
[6]J. E. Inglesfield, J. Phys. C **11**, L69 (1978); **12**, 149 (1979).
[7]H. Krakauer, M. Posternak, and A. J. Freeman, Phys. Rev. Lett. **43**, 1885 (1979).
[8]A. Fasolino, G. Santoro, and E. Tosatti, Phys. Rev. Lett. **44**, 1684 (1980); C. Z. Wang, A. Fasolino, and E. Tosatti, Surf. Sci. **211-212**, 323 (1989).
[9]M. Posternak, H. Krakauer, A. J. Freeman, and D. D. Koelling, Phys. Rev. B **21**, 5601 (1980).
[10]L. F. Mattheiss and D. R. Hamann, Phys. Rev. B **29**, 5372 (1984).
[11]C. L. Fu, A. J. Freeman, E. Wimmer, and M. Weinert, Phys. Rev. Lett. **54**, 2261 (1985).
[12]K. Terakura, I. Terakura, and Y. Teraoka, Surf. Sci. **86**, 535 (1979).
[13]M. Weinert, A. J. Freeman, and S. Ohnishi, Phys. Rev. Lett. **56**, 2295 (1986).
[14]S. Ohnishi, A. J. Freeman, and E. Wimmer, Phys. Rev. B **29**, 5267 (1984).
[15]G. Tréglia, M-C. Desjonqueres, and D. Spanjaard, J. Phys. C **16**, 2407 (1983).
[16]D. W. Bullett and P. C. Stephenson, Solid State Commun. **45**, 47 (1983); P. C. Stephenson and D. W. Bullett, Surf. Sci. **139**, 1 (1984).
[17]D. Singh and H. Krakauer, Phys. Rev. B **37**, 3999 (1988).
[18]L. D. Roelofs, T. Ranseyer, L. L. Taylor, D. Singh, and H, Krakauer, Phys. Rev. B **40**, 9147 (1989).
[19]X. W. Wang and W. Weber, Phys. Rev. Lett. **58**, 1452 (1987); X. W. Wang, C. T. Chan, K. M. Ho, and W. Weber, *ibid.* **60**, 2066 (1988).
[20]L. W. Swanson and L. C. Crouser, Phys. Rev. Lett. **16**, 389 (1966).
[21]B J. Waclawski and E. W. Plummer, Phys. Rev. Lett. **29**, 783 (1972).
[22]B. Feuerbacher and B. Fitton, Phys. Rev. Lett. **29**, 786 (1972).
[23]S. L. Weng, E. W. Plummer, and T. Gustaffson, Phys. Rev. B **18**, 1718 (1978); S. L. Weng, T. Gustaffson, and E. W. Plummer, Phys. Rev. Lett. **44**, 344 (1980).
[24]J. C. Campuzano, D. A. King, C. Somerton, and J. E. Inglesfield, Phys. Rev. Lett. **45**, 1649 (1980); J. C. Campuzano, J. E. Inglesfield, D. A. King, and C. Somerton, J. Phys. C **14**, 3099 (1981).
[25]M. I. Holmes and T. Gustafsson, Phys. Rev. Lett. **47**, 443 (1981).
[26]W. Drube, D. Straub, F. J. Himpsel, P. Soukisssian, C. L. Fu, and A. J. Freeman, Phys. Rev. B **34**, 8989 (1986).
[27]I. L. Krainsky, J. Vac. Sci. Technol. A **5**, 735 (1987).
[28]B. Salanon and J. Lapoujoulade, Surf. Sci. **173**, L613 (1983).
[29]H.-J. Ernst, E. Hulpke, and J. P. Toennies, Phys. Rev. Lett. **58**, 1941 (1987); Europhys. Lett. **10**, 747 (1989); E. Hulpke and D.-M. Smilgies, Phys. Rev. B **40**, 1338 (1989).
[30]I. K. Robinson, A. A. MacDowell, M. S. Altman, P. J. Estrup, K. Evans-Lutterodt, and R. J. Birgeneau, Phys. Rev. Lett. **62**, 1294 (1989).
[31]I. Stensgaard, L. C. Feldman, and P. J. Silverman, Phys. Rev. Lett. **42**, 247 (1979).
[32]E. K. Schweizer and C. T. Rettner, J. Vac. Sci. Technol. A **7**, 1937 (1989).
[33]K. E. Smith, G. S. Elliott, and S. D. Kevan, Phys. Rev. B **42**, 5385 (1990).
[34]J. A. Wilson, F. J. Disalvo, and S. Mahajan, Adv. Phys. **24**, 117 (1975).
[35]W. K. Han and S. C. Ying, Phys. Rev. B **41**, 4403 (1990); **41**, 9163 (1990).
[36]P. J. Estrup, I. K. Robinson, and J. C. Tully, Surf. Sci. **215**, L297 (1989).
[37]J. C. Tully (private communication).
[38]K. E. Smith and S. D. Kevan, Phys. Rev. B **43**, 1831 (1991).
[39]S. D. Kevan, Rev. Sci. Instrum. **54**, 1441 (1983).
[40]P. Thiry, P. A. Bennett, S. D. Kevan, W. A. Royer, E. E. Chaban, J. E. Rowe, and N. V. Smith, Nucl. Instrum. Methods **222**, 85 (1984).
[41]R. H. Gaylord, K. Jeong, and S. D. Kevan, Phys. Rev. Lett. **62**, 2036 (1989); K. Jeong, R. H. Gaylord, and S. D. Kevan, Phys. Rev. B **39**, 2973 (1989); R. H. Gaylord, K. Jeong, S. Dahr, and S. D. Kevan, J. Vac. Sci. Technol. A **7**, 2203 (1989).
[42]E. W. Plummer and W. Eberhardt, *Advances in Chemical Physics* (Wiley, New York, 1982), Vol. 49.
[43]F. J. Himpsel, Adv. Phys. **32**, 1 (1985).
[44]M. Prutton, *Electronic Properties of Surfaces* (Hilgar, Bristol, 1984).
[45]M. S. Hybertsen and S. G. Louie, Phys. Rev. Lett. **55**, 1418 (1985); Phys. Rev. B **34**, 5390 (1986).
[46]D. A. Papaconstantopoulos, *Handbook of the Band Structure of Elemental Solids* (Plenum, New York, 1986).
[47]F. Herman and S. Skillman, *Atomic Structure Calculations* (Prentice-Hall, Englewood Cliffs, NJ, 1963).

[48]R. F. Girvan, A. V. Gold, and R. A. Phillips, J. Phys. Chem. Solids **29**, 1485 (1968).
[49]G. S. Elliott, K. E. Smith, and S. D. Kevan, Phys. Rev. B **43**, 3893 (1991).
[50]Wei Di, K. E. Smith, and S. D. Kevan, Phys. Rev. B **43**, 12 062 (1991).
[51]M. Tomasek and S. Pick, Surf. Sci. L **279**, 140 (1984); Czech. J. Phys. B **35**, 768 (1985); Physica B **79**, 132 (1985); S. Pick, M. Tomasek, and M. U. Luchini, Chem. Phys. Lett. **164**, 345 (1989).
[52]H. C. Longuet-Higgins, U. Opik, M. H. L. Pryce, and R. A. Sack, Proc. R. Soc. London Ser. A **244**, 1 (1958).
[53]R. E. Peierls, *Quantum Theory of Solids* (Oxford University, London, 1974).
[54]J. M. Ziman, *Principles of the Theory of Solids* (Cambridge University, Cambridge, 1972).
[55]A. W. Overhauser, Phys. Rev. **128**, 1437 (1962).
[56]S.-K. Chan, and V. Heine, J. Phys. F **3**, 795 (1973).